Int j simul model 24 (2025) 1, 87-98
Original scientific paper

REFLOW PROCESS OPTIMIZATION OF TINNED COPPER STRIP BASED ON FSI-THERMAL SIMULATION

San, Y. L.[*,**]; Zhang, C. Y.[*]; Zhong, F.[*]; Qie, L. L.[*,#] & Liu, Y. B.[***]

[*] School of Mechanical Engineering, Hubei Engineering University, Xiaogan 432000, China

[**] Hubei Engineering Research Center for Key Technologies in Modern Paper and Sanitary Products Manufacturing, Xiaogan 432000, China

[***] Key Laboratory of Modern Agricultural Equipment and Technology, Ministry of Education, Jiangsu University, Zhenjiang 212013, China

E-Mail: qieliang1010@163.com ([#] Corresponding author)

Abstract

The reflow process of tinned copper (TC) strips is critical for meeting the high metal surface quality standards in electronic devices. A significant challenge is obtaining high-quality reflow-derived tinned copper (R-TC) through the remelting of the tin layer. The fluid–solid thermal (FSI-Thermal) coupling in this process is crucial for tin plating quality. This study proposes an effective method to address local yellowing on the R-TC surface by developing an FSI-Thermal model and optimizing the reflow process. At the feed rate of 0.1 m/s, heat flow of 925 K, and inlet velocity of 10 m/s, the force borne on the TC surface is even, and the minimum temperature approaches 532.4 K (> 505.05 K), accompanied by the thermal stress-induced deformation. However, the TC surface temperature is distributed unevenly in the external chamber. Reflow test is performed based on simulated parameters. Results show that due to the thickness difference of surface oxides, local yellowing takes place on the R-TC surface, and the optimized reflow process substantially reduces the nonuniformity of the tinned oxide layer and realizes the high-quality sedimentation of the clad layer.

(Received in October 2024, accepted in February 2025. This paper was with the authors 3 weeks for 2 revisions.)

Key Words: Reflow, Tinned Copper, Reflow-Derived Tinned Copper, Fluid-Solid Thermal, Process Optimization

1. INTRODUCTION

Composite metal materials have been widely used in the electronic field because of their corrosion resistance and electrical conductivity [1]. Problems such as poor interface bonding and stress concentration between different materials occur, which leads to the decline of material properties and even result in safety problems [2]. Tinned copper (TC) is a common type of composite metal material. Generally, copper strip is used as the substrate, and tin matte or bright tin is electroplated on the surface of copper by electroplating. The most evident problem in electroplating is that tin whiskers with conductivity are formed, which causes electronic short circuit and even the fault or failure of electronic devices. The research shows that compressive stress is the main reason for the growth of tin whiskers [3]. Reflow process can effectively eliminate the internal stress produced in copper strip electroplating, inhibit the formation of tin whiskers on the surface, and help avoid the short circuit fault of electronic equipment components [4]. Fig. 1 shows that under the initial state of high-temperature remelting in the reflow process, an oxide layer is formed on the surface of the matte tin, and a diffusion layer is formed at the junction of the tin layer and copper layer; then, the additives in the matte tin move toward the oxide layer and form tin crystal nuclei on the diffusion layer; finally, the tin crystal nucleus gradually becomes larger, and after cooling, a bright tin surface is produced [5]. Reflow process, as an efficient metal surface heat treatment technology, has been widely used in tin plating on copper strip surface [6].

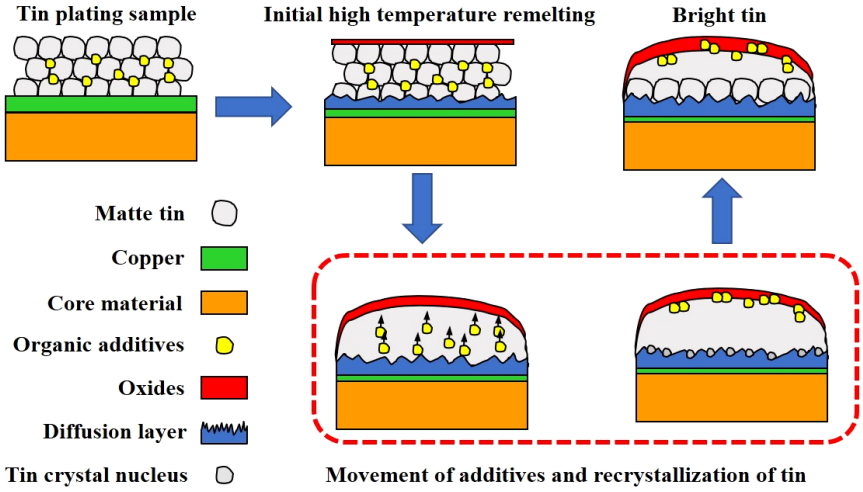

Figure 1: Reflow process analysis.

As increasingly higher requirements have been proposed by e-enterprises for TC material surface quality, the structural design of heat treatment equipment has matured, and reflow technology has become the core technology to improve production quality [7]. The surface quality of TC directly affects the electrical conductivity, weldability, and corrosion resistance of products [8]. As for the improvement of metal surface quality, traditional methods usually rely on electroplating, coating, heat treatment, and other processes, and optimization has been realized through repeated experiments [9-11]. However, these methods have limitations. An extremely low current density in electroplating leads to a loose coating structure and increased internal stress, whereas an exceedingly high current density gives rise to rough or burnt coating, and the metal ion concentration, pH, temperature and additives in the plating solution need to be adjusted and analysed regularly, which consumes excessive manpower and material resources [12]. Achieving a uniform distribution of coating is difficult, especially on workpieces with complex shapes, which leads to uneven coating thickness or missing coating [13]. High-temperature operation in heat treatment involves safety risks, including fire, scald, and equipment failure, and even produces harmful gases that pollute the environment [14]. When these traditional processes are applied to improve metal surface quality, the research and development cost becomes high with a long cycle. In the auxiliary analysis by simulation, physical phenomena are generally simulated by mathematical models and computer programs, and studies investigated the overall behaviour of complex systems and the interaction between their internal subsystems [15], but the influences of heat flow on the heat exchange and stress condition of moving metals have been rarely analysed through multifield coupling simulation. Therefore, the heat exchange law of TC in the heat flow field is simulated via simulation software, and the influence of the reflow process on TC is discussed to improve the surface properties of TC.

In view of the above problems, related remelting devices have been modelled and analysed [16], yet the analysis and research on the influence of the coupling relationship between heat flow and TC on the remelting and recrystallization state of the tin layer on TC surface are lacking. Therefore, accurately predicting the influence of hot air on TC in the reflow process is urgent. In this study, the reflow process of TC is simulated by fluid–solid–heat coupling, and the heat exchange law of TC moving in hot air field is analysed. To address the yellowing of reflow-derived tinned copper (R-TC), research and optimization are performed, and defect-free R-TC is obtained. A fluid–solid thermal (FSI-Thermal) model is established for fluid–solid–heat three-phase coupling analysis aiming at the reflow process of TC to provide a scientific basis for optimizing process parameters. This study can provide theoretical guidance and practical reference for the secondary treatment of TC.

2. STATE OF THE ART

During metal processing, high-precision modelling and analysis are generally conducted by software and computer simulation technology [17]. Hassan and Jawad [18] established a multioutput artificial neural network model through MATLAB software to predict the quenching and tempering temperatures of martensitic stainless steel and compared the results with those of regression analysis. However, the dynamic changes in heat treatment were ignored, and the model could not be accurately predicted. Schuppener et al. [19] combined Abaqus FEA software and MatCalc software to verify and calculate various local microstructure characteristics, and optimized functions using fitting test data. However, the model was not simplified enough, and the calculation workload was large. Kuang et al. [20] used COMSOL software to simulate the wettability of liquid droplets on the hydrophobic layer of metal surface and obtained a multifunctional superhydrophobic surface on aluminium alloy by laser etching technology. Nevertheless, the calculation model was not verified.

Coupling simulation is a widely used method for model prediction when metal processing involves the interaction of multiple physical fields [21]. Ren et al. [22] performed copper cold spraying outside the cavity by continuous wave process and established the electromagnetic thermal coupling simulation model of superconductor cavity for verification. However, uncertainties in system parameters and errors in the results were observed. Santos et al. [23] integrated the Hall–Petch model with the Ludvig model to simulate and predict the alloy heat and microstructural parameters produced by solidification in metal moulds, determined the equations for the solidification time and cooling rate of castings, and obtained the average error of ultimate strength of front and rear wheels. However, differences were observed between experimental conditions and actual working conditions, which influenced the effectiveness of verification. Doubiani et al. [24] studied a new eddy current model of heavy metals based on volume coupling, assumed a probability density function, introduced a step function to solve the randomness of linear eddy current, and proved that multiple linear eddy currents first affected the scalar value distribution in the computational fluid dynamics domain. Due to the influence of turbulent interaction, some model data substantially differed from the experimental results.

In addition, by optimizing the model and parameters, the process of metal treatment can be effectively optimized, and the production efficiency and quality of products can be improved [25]. With the help of convolutional neural networks and metal particle swarm optimization algorithms of Gaussian process, Yan et al. [26] automatically optimized the parameters and proposed an activation function to improve the performance parameters of the model and ensure its convergence rate, but did not conduct research and analysis combining the actual working conditions. Alam and Ali [27] optimized the elasticity of products by using a dynamic inoperable input–output model and nonlinear optimization technology, but the related research was not sufficient and lacked practicality. Paramasivam et al. [28] optimized the process by fitting the adsorption kinetics with the quasi-second-order dynamic model and compared the isothermal model and the Temkin model to predict the process conditions. The theoretical model needs to be linearized to fit the experimental data, which, however, will introduce errors.

Among the above studies, modelling analysis, model comparison, or parameter optimization have been mainly adopted, but experimental verification and optimization analysis, not to mention the related research on multifield coupling in the heat treatment of metals, are rarely involved. In this study, the coupling simulation model of TC and heat flow interaction is established using FSI-Thermal coupling simulation to predict the potential problems triggered by the thermal stress and fluid–solid interaction. Starting from theoretical calculation and modelling, the fluid–solid–heat interaction of TC in the heating chamber is

discussed and analysed, and tests are performed to verify the simulation results and to provide reference for optimizing the reflow process of TC.

The remainder of this study is organized as follows: Section 3 describes the physical and mathematical models of the matte tin remelting device and heating chamber, analyses and densifies model grids, and studies the FSI-Thermal coupling model method. Section 4 analyses and discusses simulation results, implements experimental verification, presents causes of TC surface yellowing, optimizes the reflow process, and acquires high-quality R-TC. Section 5 draws conclusions and discusses the limitations and opportunities for future work.

3. METHODOLOGY

3.1 Physical models

To verify the practicability and effectiveness of the matte tin hot air remelting device, the matte tin hot air remelting device produced by Dongguan Yichuang Surface Treatment Technology Company Limited was used to assess the performance of the designed matte tin remelting mechanism. The core part of the test device was the matte tin hot air remelting mechanism, which included three main components: heating chamber, heating system, and cooling system. The heating chamber, which was the most important structure of the matte tin remelting device, was designed with a double-layer (inner and outer) structure, where the outer chamber was divided into three parts and the inner one had dimensions of 300 mm × 600 mm × 180 mm. A thermal insulation layer was added based on the inner chamber to improve the heating efficiency. Figs. 2 a and 2 b show that the heating chamber was set with TC strip inlets and outlets, including seven air intakes and two air outlets.

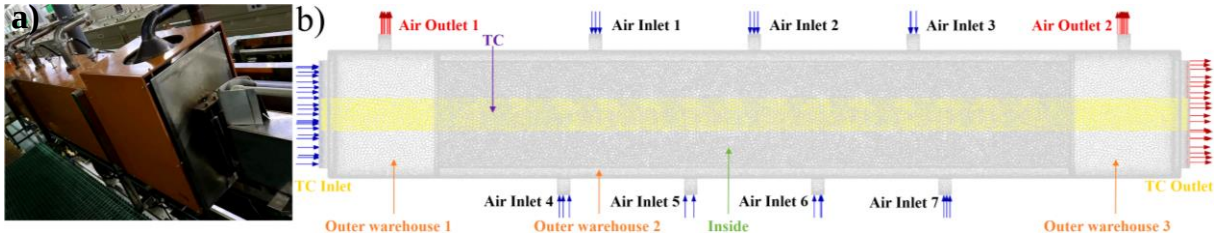

Figure 2: Schematic diagram of the physical model: a) physical model, b) grid model.

Table I: Material properties.

Material properties	304 Stainless Steel	Cu	Sn
Modulus of elasticity (E/GPa)	200	117	75
Bulk density ($kg \cdot m^{-3}$)	7930	8960	7280
Thermal conductivity ($W \cdot m^{-1} \cdot K^{-1}$)	18.5	401	67
Specific heat capacity ($J \cdot kg^{-1} \cdot K^{-1}$)	500	385	220
Poisson's ratio	0.3	0.34	0.27
Coefficient of expansion ($10^{-6}\ K^{-1}$)	16.75	17	29
Melting point (K)	1723.15	1358.15	505.05

Different kinds of TC can be produced by different electroplating processes, which can be largely divided into two types: matte tin and bright tin. In the test, the material used was the copper strip with standard dimensions, and a matte tin layer was preplated on the surface. The TC was 150 mm in width and 1 mm in thickness to simulate the workpiece in actual production. During the metal surface treatment, simulation software has been widely applied for modelling and analysis. In Workbench interface, the model was imported into FLUENT and Static Structural (SS) modules, and relevant parameters were set. The wall of the heating chamber was made of 304 stainless steel, and its relevant parameters are listed in Table I.

3.2 Mathematical model

The simulation parameters set for the fluids with different compression properties vary. According to Mach number, fluid can be divided into compressible fluid and incompressible fluid, and calculated according to Eq. (1).

$$M_a = \frac{V}{C} = \frac{V}{165.8 + 0.606T} \tag{1}$$

where M_a is the Mach number of fluid; V is the wind velocity inside the heating chamber, m/s; C is the sound propagation speed, m/s; T is the temperature at the air intake of the heating chamber, K.

The structural parameters of the heating chamber were substituted into Eq. (1), and M_a was calculated to be 0.02 (< 0.3), which indicates that the hot air fluid in the heating chamber was incompressible gas fluid. The Reynolds number of flowing viscous gas must be calculated to determine its flow state, namely, laminar flow or turbulent flow, as shown in Eq. (2).

$$Re = \frac{\rho v L}{\mu} \tag{2}$$

where ρ is the fluid density, kg/m^3; v is the average wind velocity of hot air in the heating chamber, m/s; L is the pipe diameter, m; μ is the viscosity coefficient of hot air.

The relevant parameters of gas in the heating chamber were substituted into Eq. (2) to obtain Re value was 107569, which was higher than the critical value 2,000, so the hot air fluid in the heating chamber was turbulent flow and the k-ε turbulence model was adopted.

3.3 Analysis of grid and local encryption

The discretization of the wind field model was the basis of fluid mechanics analysis, and the geometric shape was transformed into a calculation model that could participate in the numerical analysis, that is, the heating chamber grids were divided into expansion meshes and surface meshes during grid division. The heating chamber was divided into unstructured tetrahedral grids, and the average size of the global grids was 0.015 m. In the TC matte tin remelting, the physical phenomena of material inlet and outlet, air inlet and air outlet are particularly complicated, and higher grid density is needed to capture the changes in these areas accurately. Therefore, implementing local densification in these key areas is very necessary. The simulation area was divided into several sub areas, and according to the characteristics of reflow phenomena, densification was implemented at the inlet, outlet, and inner chamber. The grids in the near-wall area were locally densified, five boundary layers were added to the fluid–solid interface, the first-layer grids were 0.001 m in thickness, y+ value was kept smaller than 1, and the grid growth rate of the local densification area was kept within 1.1. The network model included about 4.3 million grids, 128,742 nodes, and 408,527 elements. The grid quality inspection showed that the mean value of grid orthogonality was 0.92, the length–width ratio was smaller than 5:1, and the distortion was smaller than 0.8, which meet the standard of high-quality grids.

3.4 FSI-Thermal coupled model

The remelting of the TC matte tin layer was simulated and analysed by using the FSI-Thermal coupling method. The model was imported into Workbench for grid division and densification, and the TC and hot air field models were constructed. Relevant parameters were set in Fluent and calculated by energy equation; the k-ε model was used as the viscosity model, the air inlet was used as the velocity inlet boundary, the air outlet was used as the velocity outlet boundary, the strip inlet was used as the quality inlet boundary, and the strip outlet was

used as the quality outlet boundary. The moving speed of TC strips was set to 0.1 m/s, the inlet heat flow was 10 m/s and 925 K, and the outlet was -10 m/s. First, the steady-state calculation was conducted, and after 100 iterations to stabilize the flow field, the transient calculation with mixed initialization was performed. The time step of the heating chamber was set to 1×10^{-2} s in Fluent, and the data were imported into the SS module after solving. The strip parameters were set in the SS module, the strip grids were redivided, the temperature distribution results obtained in Fluent were mapped to the corresponding surface in the SS module as the temperature load, and the constraint conditions were set and analysed. Fig. 3 displays the FSI-Thermal coupling simulation analysis. Through the design and construction of the above test device, this study can comprehensively evaluate the performance of the matte tin hot air remelting mechanism and provide a scientific basis for the further optimization and practical application.

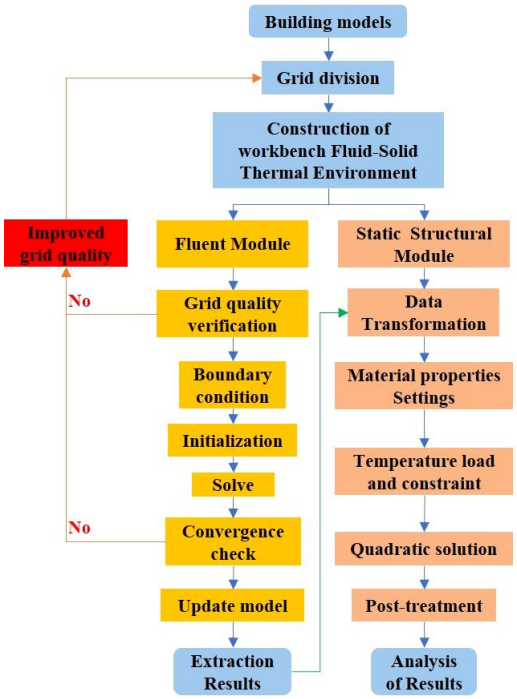

Figure 3: FSI-Thermal coupling flow diagram.

4. RESULTS ANALYSIS AND DISCUSSION

4.1 FSI-Thermal coupling analysis

According to the existing matte tin remelting device, the remelting and recrystallization of TC in the heating chamber of the 925 K and 10 m/s hot air field at the speed of 0.1 m/s was studied. The pressure and temperature cloud maps of the flow field as well as the pressure, temperature, and thermal stress distributions of TC in the hot air field were acquired.

The reflow process was analysed in Fluent. Fig. 4 a shows that due to the fluid acceleration and thermal expansion effect, the pressure at the air inlet and the outer chamber was high, and it dropped rapidly after entering the inner chamber, which resulted in a pressure difference between the inner and outer chambers. The outer and inner chambers were connected by 14 inner air inlets, and when the hot air passed through the inner air inlet, the temperature and pressure were dispersed. At the air outlet, the fluid began to gather in this area and was ready to be discharged, and the pressure dropped suddenly. Fig. 4 b shows that the TC temperature in the inner chamber could exceed 550 K, the temperature distribution in the heating chamber was uniform, and the heat conduction coefficient on the TC surface was quite different from

the convective heat transfer coefficient of the fluid, which led to the zigzag change at the junction in the temperature cloud map.

Fig. 5 a shows that the pressure generated by the hot air in the inner chamber was evenly distributed on the surface of TC, which could promote the flow of molten tin, and contribute to the remelting, recrystallization, and filling of minute pits and gaps on the surface of the substrate. According to the Fourier law of heat conduction, under certain pressure, the contact area inside the material increases and improves the heat conduction efficiency. If the pressure distribution is uneven, the local thermal conductivity becomes different, which affects the melting rate and uniformity of the tin layer. Fig. 5 b shows that the surface temperature of TC could reach the melting temperature of matte tin, and the surface temperature distribution at the inner chamber was uniform. The temperature difference between the inlet and outlet reveals that the heat preservation effect in the heating chamber was satisfactory, and the cooling rate at the outlet was fast, which could effectively promote the remelting and recrystallization of TC, but the boundary temperature of TC after leaving the inner chamber was slightly higher than that in the middle area. Fig. 5 c presents that TC experienced minor deformation under the action of thermal load, and the inner chamber was deformed greatly.

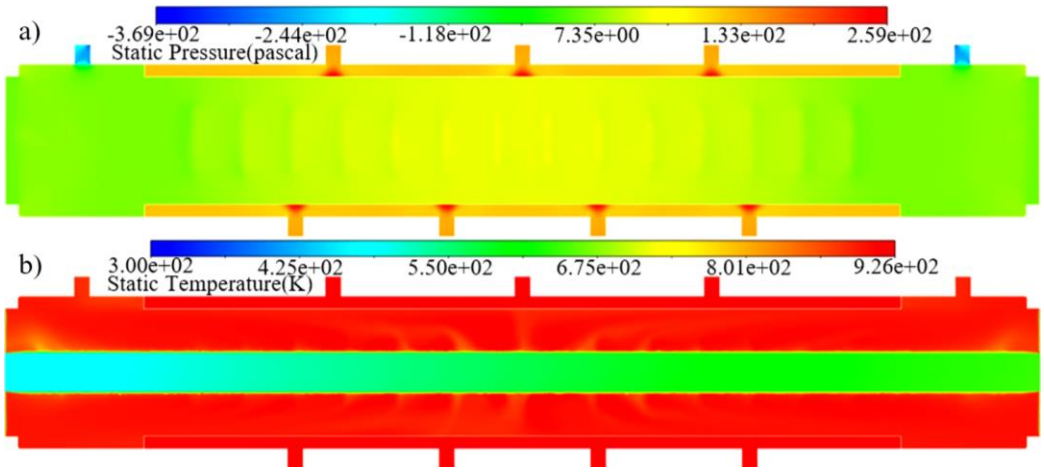

Figure 4: FLUENT simulation cloud image: a) pressure distribution, b) temperature distribution.

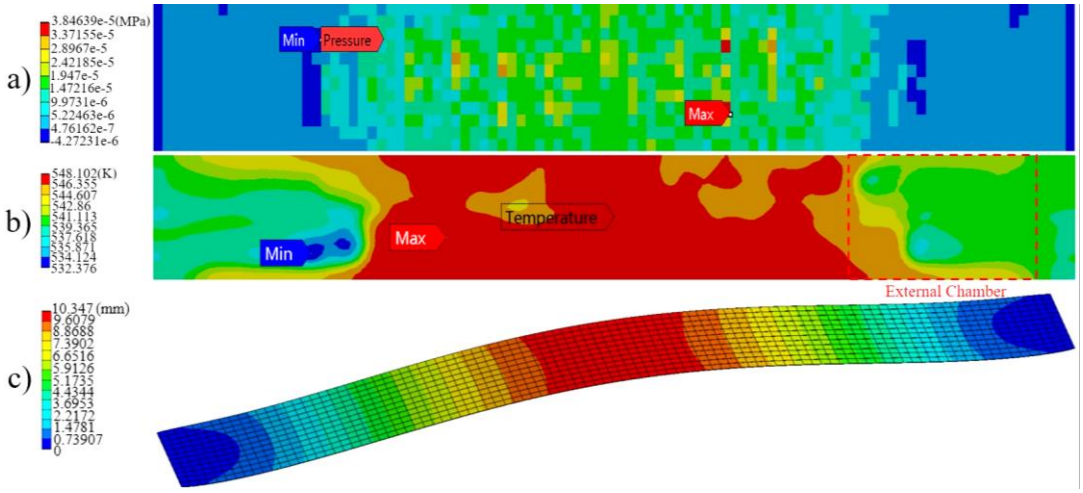

Figure 5: SS distribution cloud: a) temperature cloud, b) pressure cloud, c) total deformation distribution diagram.

At the speed of 0.1 m/s, TC entered the heating chamber with 925 K heat flow and inlet and outlet velocity of 10 m/s for the reflow process. Pressure and temperature were distributed evenly on the product surface.

4.2 Reflow test analysis

Evident differences were observed in surface quality between unremelted TC after electroplating and R-TC after the reflow process. Figs. 6 a and 6 b show many granular sediments on the surface of the unremelted sample after electroplating, along with very small holes, which indicate poor surface properties. The reflow process was performed on TC after electroplating using the parameters determined through coupling simulation, and R-TC (Figs. 6 c and 6 d) was acquired. After remelting, no granular sediments were found on R-TC surface, which was smooth without holes, so the surface properties were improved. However, yellowing appeared on the surface of both sides after the treatment. To clarify the reasons for yellowing on the R-TC surface, the Energy Dispersive X-ray Spectroscopy (EDS) test was performed in the normal area and yellowing area, and the results are listed in Table II. The comparative analysis revealed that Sb and Zn with extremely low content were found in both areas, the two elements were of lower activity than Sn and Cu and failed to form compounds, and Sb mainly came from the electroplating additive. Thus, the two elements are not responsible for the formation of the yellowing area. To determine the reasons for the yellowing area further, the remaining Sn, Cu, O, and C in the normal area and yellowing area were subject to X-ray Photoelectron Spectroscopy (XPS) analysis, organic matter and oxide tests, and reflow optimization test, and the results are displayed in Fig. 7.

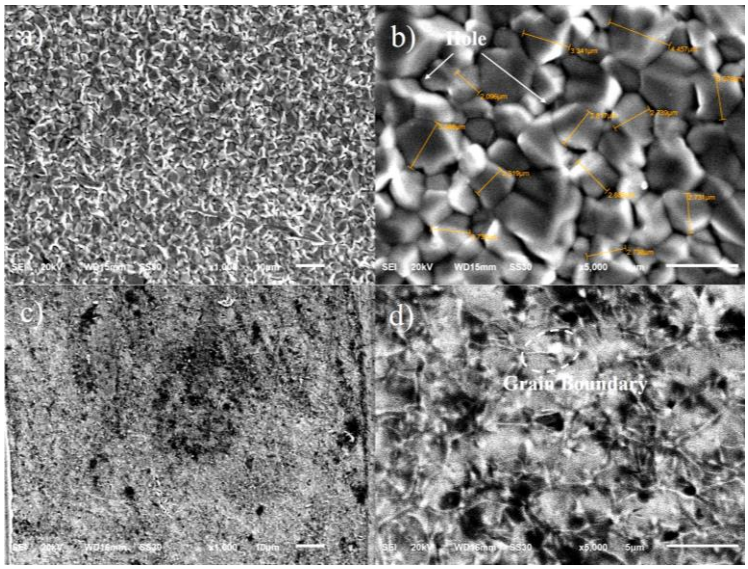

Figure 6: Electron microscopy image: a) 1000× electroplated mist tin image, b) Electroplated mist tin particles and pores, c) Matte Sn-reflow yellowing region, d) Grain boundary in yellowing region.

Table II: EDS test analysis.

		Normal region			Yellowing region		
Element	**Line type**	**Weight percentage**	***Wt* % Sigma**	**Atom percentage**	**Weight percentage**	***Wt* % Sigma**	**Atom percentage**
Sn	L-series	86.79	1.12	64.03	88.04	0.98	64.48
C	K-series	2.21	0.44	16.08	1.97	0.36	14.23
O	K-series	2.16	0.71	11.8	2.89	0.63	15.71
Cu	K-series	1.34	0.34	1.85	0.49	0.29	0.67
Zn	K-series	1.36	0.38	1.82	0.3	0.33	0.4
Sb	L-series	6.15	0.75	4.42	6.31	0.65	4.5
Aggregate		100		100	100		100

Figs. 7 a and 7 b show no evident peak signals of Cu in the two polar surface areas (within 10 nm of the surface layer), that is, no Cu was in the surface layer, which indicated that the yellowing area had nothing to do with intermetallic compounds of Cu–Sn or oxides of Cu.

The content of C in the normal area shown in Figs. 7 c and 7 d was approximately the same as that in the yellowing area. In the presence of compounds composed C element in the yellowing area, both areas should present yellow, excluding the influence of C element. As indicated in Fig. 7 e, the R-TC in the yellowing area was cut into strip samples and subjected to organic matter dissolution using methanol (MeOH), ethanol (EtOH), dimethylformamide (DMF), dimethylacetamide (DMAC) and dimethyl sulfoxide (DMSO), respectively, and then dried at 333.15 K. After that, no changes were found in the yellowing area, further excluding the influence of organic matter. Meanwhile, since pure tin does not dissolve in dilute sulfuric acid (dil. H_2SO_4), the yellowing sample was treated with dil. H_2SO_4, the colour of the yellowing area returned to normal, so the formation of the yellowing area was related to tin oxides.

Comparing the normal area (Fig. 7 f) and the yellowing area (Fig. 7 g), the peak of Sn element appeared at 495.8 eV (SnO_2) and 487.4eV (Sn), and the difference between the peak values of O element in the normal area (Fig. 7 h) and the yellowing area (Fig. 7 i) was 1.3×10^4 counts/s, which indicated that the content of SnO_2 in the yellowing area was higher, that is, the thickness of SnO_2 in both sides was greater than that in the normal area. Light interfered with the surface of SnO_2 oxide film and led to local yellowing, as shown in Fig. 7 j.

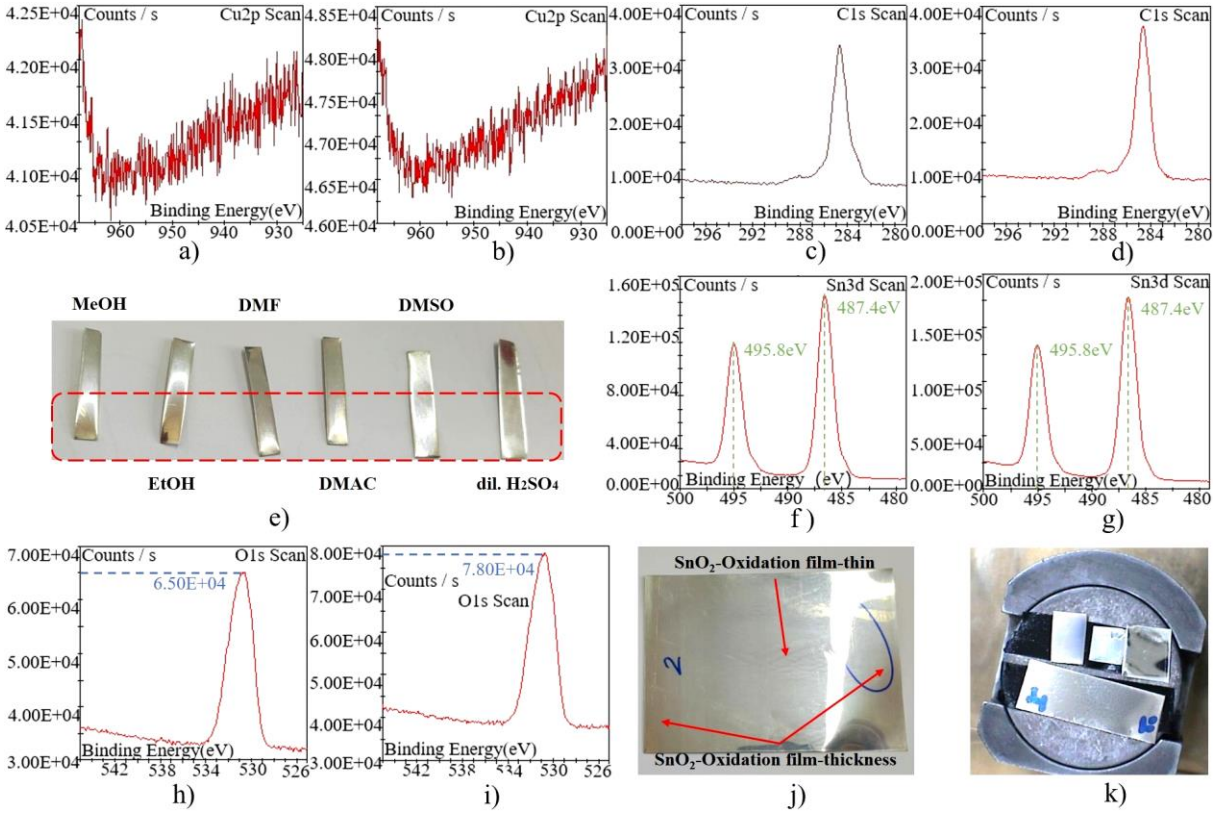

Figure 7: XPS analysis, organic and oxide testing, and reflow optimization testing: a) Normal area copper, b) Yellowing area copper, c) Normal area carbon, d) Yellowing area carbon, e) Organic verification, f) Normal area tin, g) Yellowing area tin, h) Normal area oxygen, i) Yellowing area oxygen, j) Thickness contrast, k) R-TC after reflow nitrogen treatment.

Combining the above simulation analysis and test analysis results, after TC came out of the chamber, the boundary temperature was predicted to be higher than that in the middle area. The surface area of TC was the largest in the late melting stage, and tin contacted with air

most fully, which facilitated forming an oxide layer on the surface, while more SnO_2 was generated at the boundary with higher temperature, and the uneven thickness of the oxide layer would lead to yellowing on the surface of R-TC. The distribution of defects in the experimental tin layer was consistent with the simulation analysis results. Nitrogen was introduced into the reflow process to reduce the oxygen content in the heating chamber (< 500 ppm), which could greatly reduce the production of SnO_2, eliminate the local yellowing defects on the surface, and obtain normal R-TC products, as shown in Fig. 7 k.

In the simulation mode, material properties were assumed to be evenly distributed, the molten tin flowed uniformly in the reflow process, and the chemical reaction of TC could not be specifically simulated. Microstructural nonuniformity exists in actual materials, and flow nonuniformity leads to the local nonuniform plating thickness. In the test, the R-TC surface was oxidized to different degrees. Although the simulation model could predict the TC remelting process well on the whole, differences were still found in some details. These differences were mainly induced by the simplification of model assumptions and the complexity of actual working conditions. To improve the accuracy of simulation, more actual factors should be considered in the follow-up study, and the model should be optimized and analysed.

5. CONCLUSIONS

To obtain high-quality R-TC through TC remelting based on the reflow process and to improve the stability and service life of products, an FSI-Thermal simulation model was established to simulate the remelting process of TC in the hot air field and to analyse the influence of hot air on the tin layer. The test was performed according to simulation parameters, the causes of defects were analysed, and high-quality R-TC was acquired through process optimization. Finally, the following conclusions were drawn:

(1) The simulation analysis was conducted by establishing the FSI-Thermal simulation model. The hot air passed through the outer and inner chambers to disperse the temperature and air pressure, the pressure and temperature were evenly distributed on TC surface, but the boundary temperature was higher than that in the middle area after TC came out of the inner chamber.

(2) The EDS and XPS analyses revealed that the local yellowing of R-TC surface resulted from the nonuniform thickness of SnO_2 oxide layer.

(3) Through nitrogen treatment throughout the reflow process, the thickness of SnO_2 oxide film can be greatly reduced, the nonuniformity of the tin oxide layer was remarkably reduced, and the R-TC surface became free of yellowing.

The R-TC obtained by the reflow process coincided with the simulation results. The R-TC material obtained through the improved reflow process conformed to the high-quality appearance standard within the industry.

The FSI-Thermal coupling model of the TC reflow process was proposed by combining coupling simulation with experimental verification. The model constructed according to the reflow principle was more suitable for the actual production situation and had important guiding relevance for the research on coupling simulation and process optimization. Despite the progress achieved in the coupling simulation analysis and process optimization of the matte tin remelting device, the accuracy of the FSI-Thermal model remains to be improved, and the influence of multiple factors on the reflow process needs to be analysed. In the follow-up study, the relevant factors affecting TC remelting can be more comprehensively considered and analysed to establish a multifield coupling model that more coincides with the reality for the sake of research and experimental verification.

ACKNOWLEDGEMENT

The study was supported by Science and Technology Innovation Service Project of the Hubei Provincial Department of Education Scientific Research Program (No. F2023019) and the Natural Science Foundation Project of Xiaogan (No. XGKJ2022010086).

REFERENCES

[1] Milkovic, M.; Njegovec, M.; Predan, J.; Javornik, J.; Djonlagic, D.; Gubeljak, N. (2023). Monitoring surface state of AA7075-T6 during dynamic loading with FBG sensor, *International Journal of Simulation Modelling*, Vol. 22, No. 4, 631-642, doi:10.2507/IJSIMM22-4-663

[2] Men, J.; Wang, J.; Zhang, Q.; Fan, D.; Zhou, Q.; Huang, C.-H. (2023). Experimental and numerical study on cyclic behavior of a shape-optimized composite metallic yield damper with two-phase energy dissipation, *Structures*, Vol. 53, 1012-1029, doi:10.1016/J.ISTRUC.2023.05.007

[3] Liu, Y.; Huang, M.; Chen, Y.; Liu, Y.; Zhu, Y.; Cui, L. (2023). Surface-energy-driven tin whisker growth on pure tin, *Crystals*, Vol. 13, No. 12, Paper 1643, 8 pages, doi:10.3390/CRYST13121643

[4] Li, W.; Wang, X.; Zheng, R.; Zhao, X.; Zheng, H.; Zhao, Z.; Cheng, M.; Jiang, Y.; Jia, Y. (2024). Finite element analysis of 2.5D packaging processes based on multi-physics field coupling for predicting the reliability of IC components, *Microelectronics Reliability*, Vol. 163, Paper 115530, 15 pages, doi:10.1016/J.MICROREL.2024.115530

[5] Apalowo, R. K.; Abas, M. A.; Che Ani, F.; Muhamed Mukhtar, M. A. F.; Ramli, M. R. (2024). Thermal fatigue life prediction and intermetallic compound behaviour of SAC305 BGA solder joints subject to accelerated thermal cycling test, *Soldering & Surface Mount Technology*, Vol. 36, No. 3, 154-164, doi:10.1108/SSMT-12-2023-0075

[6] Li, W.; Li, Z.; Zeng, F.-Y.; Zhang, Q.; Guo, L.; Li, D.; Ma, Y.-H.; Liu, Z.-Q. (2024). Cu pillar electroplating using a synthetic polyquaterntum leveler and its coupling effect on SAC305/Cu solder joint voiding, *Materials*, Vol. 17, No. 22, Paper 5405, 16 pages, doi:10.3390/MA17225405

[7] Lee, J. R.; Aziz, M. S. A.; Ishak, M. H. H.; Khor, C. Y. (2022). A review on numerical approach of reflow soldering process for copper pillar technology, *The International Journal of Advanced Manufacturing Technology*, Vol. 121, Nos. 7-8, 4325-4353, doi:10.1007/S00170-022-09724-W

[8] Gintrowski, G.; Reisgen, U.; Schiebahn, A.; Schmachtenberg, M.; Hibert, V. (2019). Characteristics of resistance projection–welded aluminum-copper interconnects, *Welding in the World*, Vol. 63, No. 6, 1593-1599, doi:10.1007/s40194-019-00794-1

[9] Naya, S.-I.; Nagamitsu, M.; Sugime, H.; Soejima, T.; Tada, H. (2025). Metal oxide plating for maximizing the performance of ruthenium(IV) oxide-catalyzed electrochemical oxygen evolution reaction, *Nanoscale*, Vol. 17, No. 2, 888-895, doi:10.1039/D4NR03678F

[10] Caglayan, U.; Avsar, G. (2024). Enhancing catalytic converter performance: effects of noble metals and rare earth washcoating on CO and NO_x conversion, *Research on Chemical Intermediates*, Vol. 50, No. 12, 5617-5633, doi:10.1007/S11164-024-05421-3

[11] Maniana, M.; Azim, A.; Errchiqui, F.; Tajmouati, A. (2022). Reconstruction of the thermal source from the temperature measured case of surface heat treatment of steel by laser beam, *International Journal of Heat and Technology*, Vol. 40, No. 6, 1507-1513, doi:10.18280/IJHT.400620

[12] Agrawal, V.; Mitra, B. (2023). Residual stress tuning in UV-LIGA fabricated microstructures using deposition temperature and reverse pulse plating, *Journal of Micromechanics and Microengineering*, Vol. 33, No. 3, Paper 034003, 14 pages, doi:10.1088/1361-6439/ACB3D8

[13] Le, T. S.; Chuyko, I. A.; Luchnikov, L. O.; Ilicheva, E. A.; Sukhorukova, P. K.; Balakirev, D. O.; Saratovsky, N. S.; Alekseev, A. O.; Kozlov, S. S.; Muratov, D. S.; Voronov, V. A.; Gostishchev, P. A.; Kiselev, D. A.; Ilina, T. S.; Vasilev, A. A.; Polyakov, A. Y.; Svidchenko, E. A.; Maloshitskaya, O. A.; Luponosov, Y. N.; Saranin, D. S. (2024). Tailoring wetting properties of organic hole-transport interlayers for slot-die-coated perovskite solar modules, *Solar RRL*, Vol. 8, No. 22, Paper 2400437, 7 pages, doi:10.1002/SOLR.202400437

[14] Zhao, C.; Zhao, Y.; Lin, K.; Wang, Z.; Zhou, T. (2023). Comprehensive assessment of thermal characteristics, kinetics and environmental impacts of municipal solid waste incineration fly ash during thermal treatment, *Process Safety and Environmental Protection*, Vol. 175, 619-631, doi:10.1016/J.PSEP.2023.05.074
[15] Serikov, S. V. (2024). Mathematical model of the viscoelastic medium as a method to identify metals, *Steel in Translation*, Vol. 54, No. 4, 349-354, doi:10.3103/S0967091224700748
[16] Koepf, J. A.; Gotterbarm, M. R.; Kumara, C.; Markl, M.; Körner, C. (2023). Alternative approach to modeling of nucleation and remelting in powder bed fusion additive manufacturing, *Advanced Engineering Materials*, Vol. 25, No. 12, Paper 2201682, 12 pages, doi:10.1002/ADEM.202201682
[17] Sinha, S.; Mukherjee, T. (2024). Mitigation of gas porosity in additive manufacturing using experimental data analysis and mechanistic modeling, *Materials*, Vol. 17, No. 7, Paper 1569, 18 pages, doi:10.3390/MA17071569
[18] Hassan, A. K. F.; Jawad, Q. A. (2018). Estimation of austenitizing and multiple tempering temperatures from the mechanical properties of AISI 410 using artificial neural network, *International Journal of Engineering & Technology*, Vol. 7, No. 4 (Special issue 19), 778-787, doi:10.14419/ijet.v7i4.19.27997
[19] Schuppener, J.; Berger, A.; Benito, S.; Weber, S. (2023). Simulation of local metastable microstructural states in large tools: construction and validation of the model, *The International Journal of Advanced Manufacturing Technology*, Vol. 128, Nos. 9-10, 4235-4252, doi:10.1007/S00170-023-12195-2
[20] Kuang, M.; Yang, X.; Huang, Y.; Xu, K.; Ye, X. (2023). Study on nonfluorinated preparation and properties of superhydrophobic surface, *Nano*, Vol. 18, No. 12, Paper 2350086, 14 pages, doi:10.1142/S1793292023500868
[21] Dan, Y.; Zhang, T.; Sun, X.; Dai, J.; Xu, K. (2022). Multifunctional plasmonic waveguide system based on coding metamaterials and inverse design, *Optics & Laser Technology*, Vol. 156, Paper 108478, 9 pages, doi:10.1016/J.OPTLASTEC.2022.108478
[22] Ren, M.; Lin, L.; Hao, J.; Wang, G.; Wang, Z.; Wang, D.; Shen, H.; Quan, S.; Wang, F.; Feng, L.; Jiao, F.; Zhu, F.; Zhu, K.; Yan, X.; Huang, S. (2024). Continuous wave mode test of conduction-cooled Nb_3Sn radio frequency superconducting cavities at Peking University, *Applied Sciences*, Vol. 14, No. 14, Paper 6350, 17 pages, doi:10.3390/APP14146350
[23] Santos, P. G. B. de O.; Gomes, L. F.; Spinelli, J. E. (2024). Solidification and strength behavior of A356 Al alloy wheels, *International Journal of Metalcasting*, Vol. 18, No. 4, 3609-3627, doi:10.1007/S40962-024-01286-9
[24] Doubiani, N.; Kerstein, A. R.; Oevermann, M. (2024). A pressure-coupled Representative Interactive Linear Eddy Model (RILEM) for engine simulations, *Fuel*, Vol. 355, Paper 129423, 15 pages, doi:10.1016/J.FUEL.2023.129423
[25] Campos, P. H. A.; Costa, J. F. C. L.; Koppe, V. C.; Bassani, M. A. A.; Deutsch, C. V. (2024). Short-term schedule optimization with nonlinear blending models for improved metallurgical recovery in mining, *Mining, Metallurgy & Exploration*, Vol. 41, No. 4, 1629-1643, doi:10.1007/S42461-024-00986-4
[26] Yan, H.; Zhong, C.; Wu, Y.; Zhang, L.; Lu, W. (2023). A hybrid-model optimization algorithm based on the Gaussian process and particle swarm optimization for mixed-variable CNN hyperparameter automatic search, *Frontiers of Information Technology & Electronic Engineering*, Vol. 24, No. 11, 1557-1573, doi:10.1631/FITEE.2200515
[27] Alam, I.; Ali, Y. (2023). Studying the effects of Türkiye earthquake disaster and its impact on real estate industry: a risk analysis based on input-output & non-linear optimization models, *International Journal of Disaster Risk Reduction*, Vol. 96, Paper 103920, 14 pages, doi:10.1016/J.IJDRR.2023.103920
[28] Paramasivam, S. K.; Panneerselvam, D. R.; Panneerselvam, D.; Shiva, K. N.; Subbaraya, U. (2022). Influence of operating environments on adsorptive removal of lead (Pb (II)) using banana pseudostem fiber: isotherms and kinetic study, *Journal of Natural Fibers*, Vol. 19, No. 12, 4485-4495, doi:10.1080/15440478.2020.1863295